European Journal of Pharmaceutics and Biopharmaceutics 139 (2019) 153–160

Contents lists available at ScienceDirect

European Journal of Pharmaceutics and Biopharmaceutics

journal homepage: www.elsevier.com/locate/ejpb

Research paper

Comprehensive characterization of nanostructured lipid carriers using laboratory and synchrotron X-ray scattering and diffraction

Carolin Tetyczka[a], Aden Hodzic[b], Manfred Kriechbaum[c], Krunoslav Juraić[d], Christina Spirk[a], Sonja Hartl[a], Elisabeth Pritz[e], Gerd Leitinger[e], Eva Roblegg[a,f,*]

[a] University of Graz, Institute of Pharmaceutical Sciences, Department of Pharmaceutical Technology and Biopharmacy, Universitätsplatz 1, 8010 Graz, Austria
[b] Central European Research Infrastructure Consortium (CERIC-ERIC), 34149 Basovizza, Trieste, Italy
[c] Graz University of Technology, Institute of Inorganic Chemistry, Stremayrgasse 9, 8010 Graz, Austria
[d] Ruđer Bošković Institute, Bijenička cesta 54, 10000 Zagreb, Croatia
[e] Medical University of Graz, Research Unit Electron Microscopic Techniques, Cell Biology, Histology and Embryology, Gottfried Schatz Research Center for Cell Signaling, Metabolism and Aging, Neue Stiftingtalstraße 6/II, 8010 Graz, Austria
[f] Research Center Pharmaceutical Engineering, Inffeldgasse 13, 8010 Graz, Austria

ARTICLE INFO

Keywords:
Nanostructured lipid carriers (NLC)
Palmitic acid
Laboratory small and wide angle X-ray scattering
Synchrotron X-ray diffraction
Synchrotron small angle X-ray scattering

ABSTRACT

The development of lipid nanoparticles requires knowledge on the crystalline structure, polymorphic transitions and lipid-drug interactions. This study aimed at introducing advanced techniques to characterize nanostructured lipid carriers (NLC) comprising palmitic acid, oleic acid, stabilizer and Domperidone. Crystallinity of single components and mixtures was investigated by laboratory Small Angle X-ray Scattering (SAXS). NLC were studied with laboratory Small and Wide Angle X-ray Scattering (SWAXS). Photon Correlation Spectroscopy and Freeze Fracture Transmission Electron Microscopy were used to monitor particle size, zeta potential and shape. Stability of NLC was investigated using synchrotron X-ray Diffraction (XRD) and SAXS and laboratory SAXS. Palmitic acid showed a lamellar structure (polymorph C), which was still present after particle preparation. Spherical 300 nm-sized particles with zeta potential values above −30 mV were obtained and Domperidone was incorporated in its amorphous form. During storage, no differences in synchrotron XRD spectra were seen. However, laboratory SAXS measurements showed a second lamellar structure, identified as polymorph B. Synchrotron SAXS temperature scans confirmed that polymorph B did not affect the morphology of the encapsulated drug or the shape of NLC. These results highlight the unique capabilities of laboratory and synchrotron X-ray Scattering and Diffraction for improved structural characterization of lipid nanoparticles.

1. Introduction

Self-assembled lipid nanoparticles represent alternative carriers to polymeric nanoparticles for the incorporation of lipophilic and, to a certain extent, hydrophilic drugs. They can be classified into solid lipid nanoparticles (SLN) and nanostructured lipid carriers (NLC) [1–3]. An alternative approach is the development of lipid-drug conjugate nanoparticles [4]. Here, an ionic positively or negatively charged lipid is combined with an ionic hydrophilic active, resulting in a lipophilic conjugate that is further transferred into lipid particles [5–8].

Crystalline nanoparticles are obtained when the lipid is cooled below its critical crystallization temperature [9,10]. This temperature is specific for each lipid and can be affected by the components present in the formulation (i.e., drug, surfactant etc.) [10,11]. Instead, the lipid can remain in a liquid non-crystalline emulsion state forming a so-called supercooled melt. A supercooled melt exists when the lipid is not cooled below its critical crystallization temperature and crystallizes at a temperature lower than the melting point of the lipid [9,10]. After solidification and during storage of lipid nanoparticles polymorphic changes or crystal aging phenomena might occur [10,12,13]. For example, fatty acids including stearic and palmitic acid can exist in four forms (i.e., A, B, C and E). From these four forms, only the C form crystallizes after melting [14–16]. Factors that influence the crystalline/polymorphic structure of the lipid and consequently the stability of lipid nanoparticles are the addition of matrix materials such as oils and stabilizers [10,17]. Moreover, incorporation of drugs, the manufacturing method used and storage conditions may result in alterations of the crystal lattice of the lipid [10,14,17].

* Corresponding author at: University of Graz, Institute of Pharmaceutical Sciences, Department of Pharmaceutical Technology and Biopharmacy, Universitätsplatz 1, 8010 Graz, Austria.
E-mail address: eva.roblegg@uni-graz.at (E. Roblegg).

https://doi.org/10.1016/j.ejpb.2019.03.017
Received 22 October 2018; Received in revised form 1 March 2019; Accepted 20 March 2019
Available online 21 March 2019
0939-6411/

To study these phenomena, Differential Scanning Calorimetry (DSC) and X-ray Diffraction (XRD) are the most frequently used techniques according to the literature [14]. DSC instruments enable the detection of characteristic melting or transformation endotherms upon heating (and cooling). Thereby, the presence of thermal transitions indicates crystalline or liquid crystalline particles and the absence of supercooled melts [18]. X-ray Diffraction (XRD) measures the interaction of X-ray diffraction with crystal lattices (or amorphous states) of a sample covering full wide angular range. It is utilized to identify the crystalline structure, the average nanocrystal size and the degree of crystallinity [10,18,19]. These data can be improved by using complementary tools such as Small and Wide Angle X-ray Scattering (SAXS/WAXS). X-ray scattering examines the structure of materials at nanometer and angstrom length scales [20]. WAXS is applied in angles greater than 10° and provides structural information at an atomic scale on the crystallinity of the lipid, spacing of the lipid lattice and incorporation of the drug in the lipid matrix. SAXS measurements are performed at angles between 0.1 and 10° [21]. This technique is a powerful method to understand the inner arrangement of the lipid matrix (i.e., self-assembling structure) and interactions between the drug and the lipid [10,18,19]. Moreover, SAXS spectra can be analyzed regarding the form and structure factor of nanoparticles [21]. The form factor provides structural information (i.e., size and shape) of single particles and can be determined for smaller particle sizes depending on the instrumental SAXS resolution [20,21]. Interestingly, for larger particle sizes, formed by e.g., self-assembling, the form factor can be simulated according to a core-shell function, providing information of the particle shape. The structure factor is used to determine the positional organization of particle systems [20–23].

Currently, such investigations are performed with laboratory sources. Synchrotron X-ray sources show advantages over laboratory sources because of higher X-ray beam intensity and brilliance, covering a wide range of beamline applications at reduced acquisition time and flexible sample set-ups using less sample volume. Thereby, the synchrotron beam interacts with the sample via absorption and scattering [19,24,25].

The aim of this study was to investigate the crystalline structure (i.e., fingerprints), the arrangement (i.e., self-assembling) and structural alterations such as polymorphic transitions of NLC to assess the physico-chemical stability. To this end, single components, mixtures of single components and produced NLC were analyzed using laboratory SWAXS, synchrotron XRD and SAXS. Moreover, NLC were characterized regarding particle size, zeta potential and shape.

2. Materials and methods

2.1. Materials

As poorly soluble model drug, Domperidone (Biopharmaceutics Classification System (BCS) II) was obtained from Molekula GmbH (Munich, Germany). For the preparation of NLC, palmitic acid (Merck KgaA, Darmstadt, Germany) and oleic acid (Cognis, Monheim am Rhein, Germany) were used. Tween 80 was purchased from Sigma-Aldrich (Munich, Germany). Ultrapurified water (i.e., Milli-Q®-water (MQ-water), Millipore S.A.S., Molsheim, France) was used for all experiments.

2.2. Methods

2.2.1. Sample preparation of the single components and mixtures

Single components (i.e., palmitic acid, oleic acid and Domperidone) and mixtures (i.e., binary mixture of palmitic acid and oleic acid (9:1) and ternary mixture of palmitic acid, oleic acid and Domperidone (44.1:4.9:1)) were heated to 70 °C to mimic production conditions of NLC. The samples were kept constant at 70 °C, shaken at 450 rpm for 1 h using a thermomixer comfort (Eppendorf Austria GmbH, Vienna, Austria) and stored overnight at ambient conditions. The single components including palmitic acid and an aqueous stabilizer solution of Tween 80 (2% w/w) were used without temperature treatment.

2.2.2. Preparation of NLC using high pressure homogenization

Blank and Domperidone NLC were prepared according to Tetyczka et al. [26]. Briefly, Domperidone (2% w/w; % with regard to the lipids) was mixed with the solid lipid palmitic acid and the liquid lipid oleic acid (10% w/w; ratio 9:1 of palmitic acid and oleic acid) and heated to 70 °C. Subsequently, an aqueous stabilizer solution of Tween 80 (2% w/w) was heated to the same temperature, added to the lipid mixture and stirred at 8000 rpm for 1 min using an Ultra Turrax (Ultra Turrax T25, Janke & Kunkel, IKA®-Labortechnik, IKA®-Werke GmbH & Co. KG, Staufen, Germany). The pre-suspension was transferred into a high pressure homogenizer (Panda 2 K, NS1001L Spezial, GEA Niro Soavi, Lübeck, Germany), equipped with a water jacket for temperature control. The system temperature was 70 °C during all experiments. The suspensions were homogenized running 5 cycles at 500 bar. Finally, the suspension was filled in glass vials and cooled in an ice-bath for 30 min. Blank NLC were prepared in the same way. If not otherwise stated all concentrations were given with regard to the total formulation amount.

2.2.3. Particle size and zeta potential

The particle sizes of blank and Domperidone NLC were investigated via Photon Correlation Spectroscopy (PCS) using a Zetasizer Nano ZS (Malvern Instruments, Malvern, UK) which was equipped with a 532 nm laser. The refractive indices (RI) of the investigated particles and MQ-water were set to 1.4381 (i.e., palmitic acid) and 1.3325, respectively. The measurements were performed at 25 °C with an equilibration time of 30 sec and a measurement angle of 173° (backscatter). PCS yields the polydispersity index (PdI) as a measure of the width of the particle size distribution and the hydrodynamic diameter (z-average).

The zeta potential was assessed via Laser-Doppler-Electrophorese coupled with PCS (Zetasizer Nano ZS, Malvern Instruments) using a scattering angle of 173° at 25 °C. The calculation was performed according to the Helmholtz-Smoluchovski equation [27]. Prior to measurements, samples were diluted in zeta-water (i.e., distilled water adjusted with 0.9% (w/v) sodium chloride solution to a conductivity of 50 μS/cm and a pH of 5.5–6).

2.2.4. Visualization of NLC by freeze fracture transmission electron microscopy (TEM)

The samples were frozen in liquid propane before being stored in liquid nitrogen. Fractures were created in a Balzers BAF400D freeze-etching apparatus (Leica Camera AG, Wetzlar, Germany) under vacuum (pressure between 1.3×10^{-4} and 1.3×10^{-5} Pa). The surfaces of the fractures were coated with platinum (i.e., film thickness of 20 nm applied at 30°) and carbon (i.e., film thickness of 200 nm applied at 90°) to produce replicas. The replica thickness was controlled using a quartz crystal thin-film monitor. The replicas were cleaned using sodium hypochlorite solution, stored in 50% NaOH and washed three times with distilled water. Next, the samples were mounted on an uncoated copper grid and visualized using a TECNAI 20 with a Transmission Electron Microscopy (TEM) Detector (FEV Thermo Fisher, Eindhofen, Netherlands) equipped with a Gatan US1000 camera operated at an acceleration voltage of 120 kV.

2.2.5. Laboratory SAXS and WAXS

Samples were filled into glass capillaries (diameter of 2 mm), sealed with wax, and placed into an Anton Paar capillary sample holder. For sample analysis, a high-flux SAXSess camera (Anton Paar, Graz, Austria) connected with a Debye flex 3003 X-ray generator (General Electric, Frankfurt am Main, Germany) operating at 40 kV and 50 mA with a sealed-tube Cu anode was used. The Goebel-mirror focused and Kratky-slit collimated X-ray beam was line shaped (17 mm horizontal

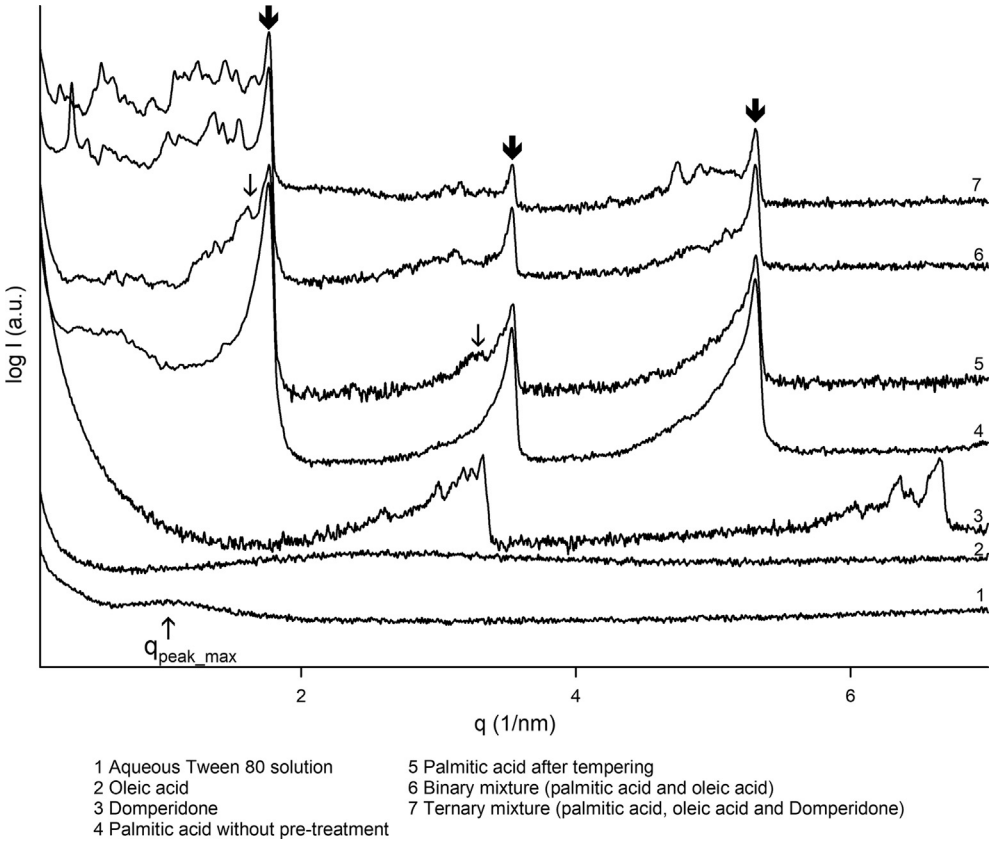

Fig. 1. Laboratory SAXS spectra of an aqueous Tween 80 solution (1). q_{peak_max} displays the scattering intensity and shows the experimental maximum (form factor) of the micelles. Laboratory SAXS spectra of oleic acid (2), Domperidone (3), palmitic acid without temperature treatment (4), palmitic acid after tempering at 70 °C for 1 h (5), binary mixture, i.e, palmitic acid and oleic acid (6) and ternary mixture, i.e., palmitic acid, oleic acid and Domperidone (7). Bold arrows show polymorph C and thin arrows denote polymorph B (i.e., second lamellar structure).

dimension at the sample position). Scattered radiation was measured in the transmission mode and recorded by a one-dimensional MYTHEN-1k micros trip solid-state detector (Dectris, Baden, Switzerland). Experiments were performed within a q-range of 0.1–5 nm^{-1}, with q being the magnitude of the scattering vector. To this end, Cu-K_α radiation of wavelength 0.154 nm and a sample-to-detector distance of 307 mm were used. This corresponds to a total 2θ region of 0.14–7°, applying the conversion q [nm^{-1}] = 4π (sin θ) /λ with 2θ being the scattering angle with respect to the incident beam and λ the wavelength of the X-rays. The d-spacing (d), also referred as lattice size, was calculated using Eq. (1),

$$d = \frac{2\pi}{q} \tag{1}$$

where q is the scattering vector. The q_{peak_max} value represents the q value at its spherical peak maximum.

2.2.6. DSC measurements of the single components and mixtures

The thermal characteristics of the single component palmitic acid with and without temperature treatment and the mixtures (i.e., binary and ternary mixture) were investigated using DSC (204F1 Phoenix, Netzsch GmbH, Selb, Germany). For this, 4–8 mg of the samples were transferred into sealed aluminum crucibles. The crucibles were pierced and purged with pure nitrogen. An empty aluminum crucible was used as reference material. Samples were heated from 4 °C to 100 °C with a heating rate of 10 K/min. After an isothermal segment at 100 °C for 5 min, samples were cooled to 4 °C with a cooling rate of 5 K/min. Purging of the DSC cell was performed with pure nitrogen at a flow rate of 20 ml/min. The data were analyzed using Proteus Thermal Analysis software (Netzsch GmbH).

2.2.7. Synchrotron SAXS Beamline

SAXS temperature scans were performed at the Austrian SAXS Beamline using synchrotron radiation source (Synchrotron Elettra, Trieste, Italy) according to Amentisch et al. [28]. Briefly, temperature scans were conducted in the temperature range from −0.15 to 69.85 °C and back to −0.15 °C, with 2 K steps. The exposure time was 30 s per frame, with an equilibration time of five s each step. The SAXS patterns obtained at the synchrotron source were analyzed and calibrations were performed with silver behenate showing a standard lattice spacing of 5.838 nm [28].

2.2.8. SAXS form factor calculation

The theoretical form factor P(q) of the spherical core-shell particle [21,29] was calculated using Eq. (2),

$$P(q) = \left[\frac{(3V_{tot} \times \rho_{shell}) \times j_1(q \times R_{tot})}{(q \times R_{tot})} - \frac{(3V_{core} \times \rho_{shell}) \times j_1(q \times R_{core})}{(q \times R_{core})} \right]^2 \tag{2}$$

where V_{tot} is the total volume of the shell, ρ_{shell} is the electron density of the shell, q is the scattering vector, R_{tot} is the outer radius of the shell, j_1 is the spherical bessel function $j_1=(\sin(x) - x(\cos(x))/x^2$, V_{core} is the volume of the core and R_{core} is the radius of the core. For the aqueous Tween 80 solution a R_{tot} of 2 nm and a R_{core} of 5 nm was used; for NLC a R_{tot} of 10 nm and a R_{core} of 100 nm was applied.

Sasview software was used for the calculation of the form factor [29].

2.2.9. Synchrotron XRD Beamline

XRD analyses were performed at the X-ray Diffraction Beamline (XRD1) of the Elettra synchrotron (Trieste, Italy) [30]. Powder diffraction patterns were collected in the transmission mode with a monochromatic wavelength of 0.1 nm (12.4 keV) and 200 × 200 μm^2 spot size, using a Pilatus 2 M hybrid-pixel area detector at 24 ± 0.5 °C. Samples were packed in borosilicate capillaries (700 µm diameter and 10 µm wall thickness). Blank samples were analyzed in the same way. The patterns were integrated using a Fit2D program [31], after

Table 1
q values and d-spacings of Domperidone, palmitic acid without temperature treatment, palmitic acid after tempering at 70 °C for 1 h, binary mixture (palmitic acid and oleic acid) and ternary mixture (palmitic acid oleic acid and Domperidone) determined via laboratory SAXS.

	q_1 (nm^{-1})	d_1 (nm)	q_2 (nm^{-1})	d_2 (nm)	q_3 (nm^{-1})	d_3 (nm)
Domperidone	3.325	1.890	6.647	0.945		
Palmitic acid without temperature treatment	1.759	3.573	3.543	1.774	5.318	1.181
Palmitic acid after tempering (polymorph C)	1.759	3.573	3.543	1.774	5.318	1.181
Palmitic acid after tempering (polymorph B)	1.586	3.961	3.286	1.912		
Binary mixture	1.759	3.573	3.543	1.774	5.318	1.181
Ternary mixture	1.759	3.573	3.543	1.774	5.318	1.181

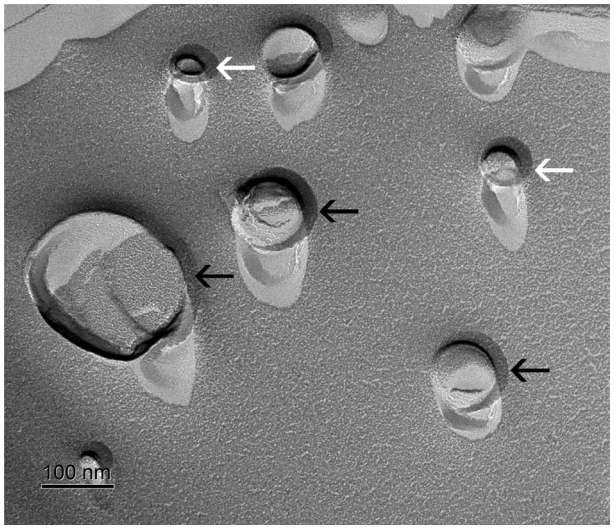

Fig. 2. A representative TEM image of Domperidone NLC. Black arrows display NLC and white arrows show micelles formed by Tween 80.

preliminary calibration of the hardware set-up, using a capillary filled with boron lanthanide (LaB_6) standard reference powder (NIST 660a).

2.2.10. Storage conditions to study physico-chemical stability

The stability of NLC was monitored for 10 weeks. To this end, particles were stored in a refrigerator (i.e., 5 ± 3 °C). The crystalline structure was analyzed after zero, four, six and 10 weeks using laboratory SAXS. Moreover, synchrotron XRD measurements were performed after zero and 10 weeks of storage. Synchrotron temperature scans were performed immediately after sample preparation and after 10 weeks of storage. All measurements were performed in triplicate.

3. Results and discussion

3.1. Results

3.1.1. Crystallinity of single components and mixtures

The crystalline structure of the single components and the mixtures was investigated via laboratory SAXS. The results are shown in Fig. 1. Table 1 summarizes the q values and d-spacings of the single components and mixtures.

SAXS spectra of the aqueous Tween 80 solution revealed an experimental maximum (q_{peak_max}) at 1.038 nm^{-1}. We fitted the data assuming a particle comprising two different electron densities and showing a diameter of 10 nm. The theoretical calculation displayed modulated maxima, which confirmed the spherical shape. The plot of the form factor analysis is provided in the supplementary material.

No crystalline structure was determined for oleic acid. By contrast, the single component Domperidone showed crystalline peaks at q_1 = 3.325 nm^{-1} and q_2 = 6.647 nm^{-1}. Palmitic acid (without pretreatment) revealed a lamellar structure (Fig. 1, Table 1) characterized by equidistantly spaced peaks. This lamellar structure can be identified as polymorph C [15,16]. After tempering of palmitic acid, a second and larger lamellar structure (long crystal spacing) was detected. This structure can be assigned to polymorph B [15].

In the binary mixture polymorph C displayed equidistantly spaced peaks; no peaks indicating the presence of polymorph B were detected. No crystalline Domperidone peaks were observed in the ternary mixture. The results indicated that Domperidone was dissolved in the lipid matrix in its amorphous form and only polymorph C was visible. The corresponding equidistantly spaced peaks were detected at q_1 = 1.759 nm^{-1}, q_2 = 3.543 nm^{-1} and q_3 = 5.318 nm^{-1}. Laboratory SAXS spectra of the binary and ternary mixture revealed additional weak signals especially at q values < 2 nm^{-1}.

Furthermore, the single components and the mixtures were monitored using DSC. Palmitic acid without temperature treatment revealed a crystallization peak at 57.4 ± 0.7 °C. After temperature treatment, the crystallization temperature slightly increased to 58.3 ± 0.9 °C. In the binary and ternary mixtures the crystallization temperature decreased to 54.8 ± 1.0 °C and 55.1 ± 0.3 °C, respectively.

3.1.2. Particle size, zeta potential and visualization of NLC

After high-pressure homogenization, particle size, particle size distribution and zeta potential of NLC (i.e., blank and Domperidone NLC) were investigated using PCS. The obtained z-average values in water were 288.28 ± 4.85 nm (blank NLC) and 301.83 ± 5.76 nm (Domperidone NLC). PdI values of 0.189 ± 0.018 (blank NLC) and 0.192 ± 0.010 (Domperidone NLC) were obtained. The zeta potential measured in zeta water was −30.57 ± 0.99 mV (blank NLC) and −32.17 ± 0.6 mV (Domperidone NLC) which coincides with Tetyczka et al. [26]. The TEM image displayed spherically shaped particles (Fig. 2, black arrows) with particle sizes of about 250 nm, which were determined as NLC. Moreover, smaller spherical structures in the size range of 10–30 nm were observed, which were identified as micelles, formed by Tween 80 (Fig. 2, white arrows). During the 10-week storage PCS data confirmed colloidal stability of the particles.

3.1.3. Crystallinity of NLC

Laboratory SWAXS measurements were used to study the crystalline structure of Domperidone, blank NLC and Domperidone loaded NLC (Fig. 3). The wide angle fingerprint area showed crystalline drug peaks of Domperidone. Blank NLC revealed a lamellar structure (i.e., peaks at q_1 = 1.759 nm^{-1}, q_2 = 3.543 nm^{-1} and q_3 = 5.318 nm^{-1} and d-spacings of d_1 = 3.573 nm, d_2 = 1.774 nm and d_3 = 1.181 nm) identified as polymorph C. The incorporation of Domperidone into NLC showed no crystalline drug peaks; only polymorph C with equidistantly spaced peaks at q_1 = 1.759 nm^{-1} (d_1 = 3.573 nm), q_2 = 3.543 nm^{-1} (d_2 = 1.774 nm) and q_3 = 5.318 nm^{-1} (d_3 = 1.181 nm) was detected. No differences were observed in SAXS and WAXS spectra of blank and Domperidone NLC.

3.1.4. Impact of morphological changes on the stability of NLC

The physico-chemical stability of blank and Domperidone NLC was investigated over a period of 10 weeks using synchrotron XRD and laboratory SAXS. Synchrotron XRD measurements were performed

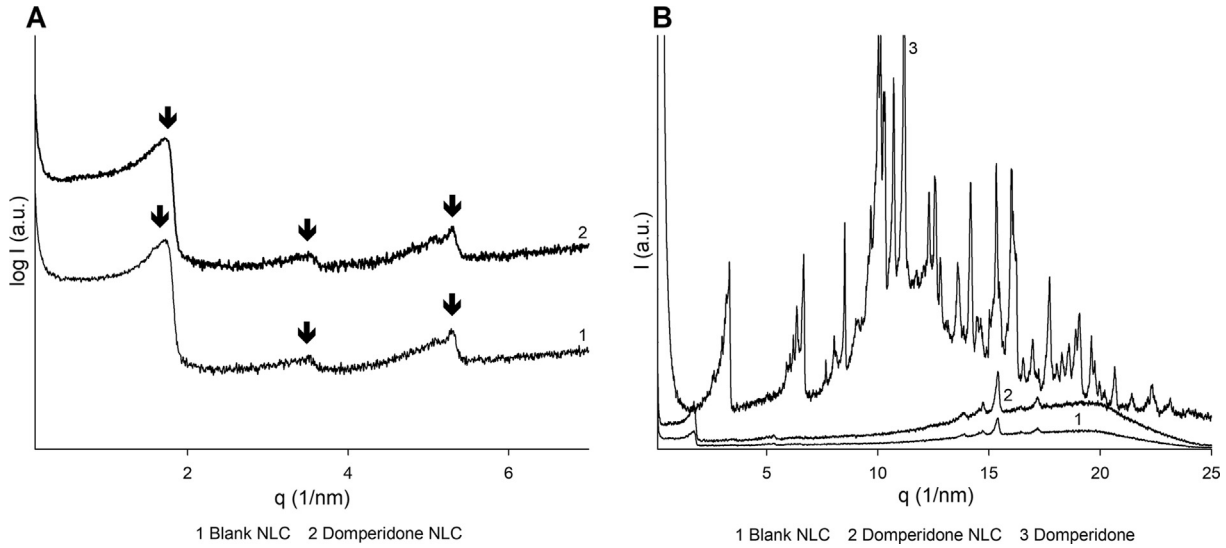

Fig. 3. (A) Laboratory SAXS spectra of blank and Domperidone NLC. Bold arrows indicate polymorph C. (B) Laboratory SWAXS spectra of Domperidone, blank and Domperidone NLC.

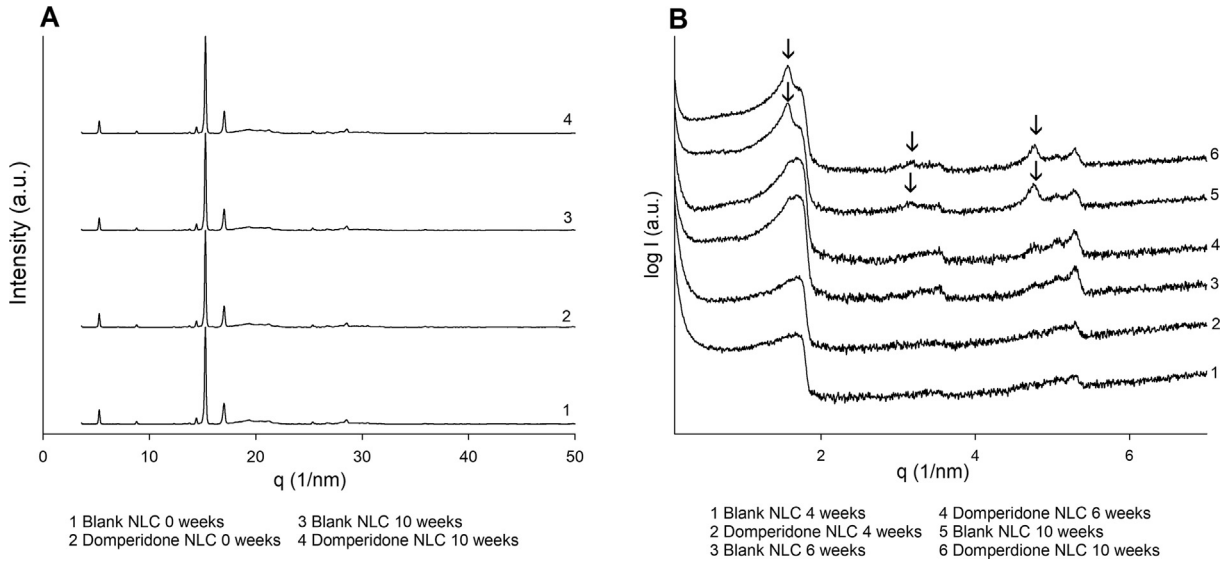

Fig. 4. (A) Synchrotron XRD spectra of blank and Domperidone NLC immediately after preparation (zero weeks) and after 10 weeks of storage. (B) Laboratory SAXS spectra of blank and Domperidone NLC after four, six and 10 weeks of storage. Arrows indicate the second lamellar structure (i.e., polymorph B).

immediately after preparation and 10 weeks after storage of NLC. Bragg peaks in the fingerprint region of the crystalline lattice were detected at $q = 5.298\,nm^{-1}$, $15.252\,nm^{-1}$ and $16.998\,nm^{-1}$ (Fig. 4A). No lamellar structure is visible in synchrotron XRD spectra, because the first peak of the spectra corresponds to the third peak in the laboratory SAXS spectra (Figs. 3A and 4A). Additionally, no differences in synchrotron XRD spectra of blank and Domperidone NLC were observed.

During storage, the crystalline structure of NLC in the fingerprint area did not change. To investigate the internal structure of blank and drug loaded lipid particles more closely, laboratory SAXS measurements (Fig. 4B) were performed. No structural changes were found after four and six weeks of storage. Equidistantly spaced peaks detected at $q_1 = 1.759\,nm^{-1}$ ($d_1 = 3.573$ nm), $q_2 = 3.543\,nm^{-1}$ ($d_2 = 1.774$ nm) and $q_3 = 5.318\,nm^{-1}$ ($d_3 = 1.181$ nm) could be assigned to polymorph C. However, additional weak signals were found in SAXS spectra of blank and Domperidone NLC. After 10 weeks of storage, a second lamellar structure with peaks at $q_1 = 1.586\,nm^{-1}$, $q_2 = 3.286\,nm^{-1}$ and $q_3 = 4.770\,nm^{-1}$ was formed (i.e., polymorph B). The lattice sizes of the second lamellar structure shifted to $d_1 = 3.961$ nm, $d_2 = 1.912$ nm and $d_3 = 1.317$ nm.

3.1.5. Synchrotron SAXS temperature scans

To study the impact of polymorph B on the particle stability during storage and assess possible aging effects, temperature scans with synchrotron SAXS were conducted (Fig. 5A). The particles transformed into an amorphous state during melting, during cooling re-crystallization occurred and particle formation took place again. After several temperature scan frames and despite the presence of polymorph B, the drug remained in its amorphous state. Equidistantly spaced peaks with d-spacing values of $d_1 = 3.573$ nm, $d_2 = 1.774$ nm and $d_3 = 1.181$ nm (i.e., polymorph C) and $d_1 = 3.961$ nm, $d_2 = 1.912$ nm and $d_3 = 1.317$ nm (i.e., polymorph B) were detected suggesting that the lamellar structure of NLC was stable. According to the scattering signal with an experimental maximum q_{peak_max} at $0.850\,nm^{-1}$ (Fig. 5A) spherically shaped particles were formed. The data were confirmed by theoretical modeling of the form factor. Since the particle sizes were beyond the instrumental resolution limit, only the scattering signal of the bilayer shell was obtained. Hence, we calculated the form factor for

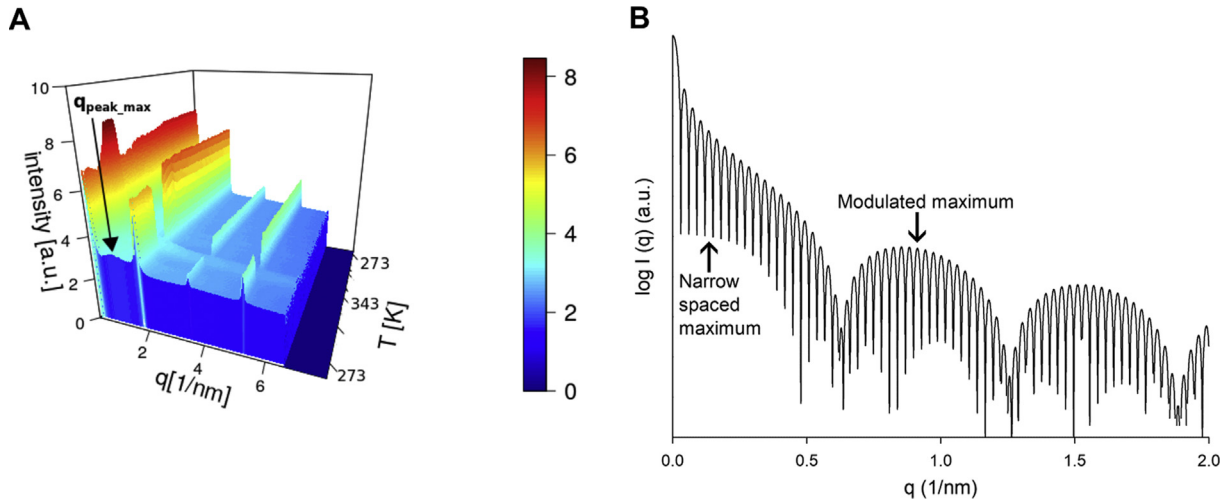

Fig. 5. (A) Representative Synchrotron SAXS temperature scan of Domperidone NLC after 10 weeks of storage from −0.15 °C (i.e., 273 K) to 69.85 °C (i.e., 343 K) and back to −0.15 °C (i.e., 273 K); q_{peak_max} displays the scattering intensity and shows the experimental maximum originating from the vesicle-bilayer thickness. (B) The simulated form factor of NLC shows the modulated maxima related to the vesicle-bilayer and the narrow spaced maxima related to the overall particle size.

a particle assuming a particle diameter of 220 nm and a shell thickness of 10 nm (Fig. 5B). The narrow spaced maxima, which corresponded to the size of the particles could not be calculated due to method limitation. The results of the simulation confirmed a spherical shape of NLC.

3.2. Discussion

Palmitic acid presented a lamellar structure with lamellar spacings of $d_1 = 3.573$ nm, $d_2 = 1.774$ nm and $d_3 = 1.181$ nm. These lamellar spacings indicate that palmitic acid was present as polymorph C [15,16]. The structure factor revealed a one-dimensional lamellar lattice, characterized by the equidistantly spaced diffraction peaks. After heating and cooling of palmitic acid, a second lamellar structure, referred to as polymorph B was formed [15,32]. According to Müller et al. tempering of lipids results in a lower ordering of the lamellar structure [33]. This suggests that heating and subsequent recrystallization of palmitic acid impacts the lamellar lattice resulting in polymorphic alterations. Similar results have also been obtained for Precirol ATO 5, a glyceryl palmitostearate, and 1-palmitoyl-2-oleyl-sn-glycero-3-phosphocholine [34,35].

Mixing palmitic acid with oleic acid (binary mixture) suppressed the formation of the thermodynamically less stable second lamellar structure [36–38] since the amorphous oil inhibited the formation of polymorphic structures [39]. Once Domperidone was added to the binary mixture, laboratory SAXS spectra showed that no crystalline peaks of the drug were observed. These results coincide with DSC data [26], confirming that Domperidone was dissolved in the lipids in its amorphous form. Consequently, the inhibition of polymorph B was further promoted due to lowering of the crystallization temperature of the lipid. The weak signals especially at q values $< 2\,nm^{-1}$ can be explained by the lower resolution of laboratory SAXS compared to synchrotron SAXS, which in turn led to an increase of the noise-level because of the line-shaped beam and smearing.

After particle preparation with high-pressure homogenization at 70 °C, blank and drug loaded NLC showed mean particle sizes of about 300 nm, a narrow particle size distribution, zeta potential values above −30 mV and an almost spherical shape. Since Tween 80 was used to stabilize NLC, it must be taken into account that Tween 80 forms micelles when the concentration is above the critical micelle concentration (CMC) [40]. The CMC value of Tween 80 is 0.018 mM (i.e., 0.002% w/v) [41], which is significantly lower than the stabilizer concentration used in this study (i.e., 2% w/w). By performing TEM and laboratory SAXS measurements, we confirmed that Tween 80 formed spherical micelles with a q_{peak_max} at $1.038\,nm^{-1}$ and sizes of about 10–30 nm. These findings are consistent with findings of comparable studies [42]. However, Laser Diffraction studies showed that after NLC production only 10% of the produced particles were below 90 nm and could be assigned to a mixture of micelles and small lipid nanoparticles. By contrast, 90% of the particles ranged from 151 to 266 nm and could be identified as NLC [26]. Consequently, during SAXS measurements the signal of larger particles (NLC) superimposed the signal of smaller particles (i.e., micelles and small lipid nanoparticles) [21].

Laboratory SAXS spectra of NLC showed broadened crystalline peaks with decreased intensity compared to the single components. This is due to the fact that the intensity of the lipid nanoparticles was reduced because of the lower amount of lipid associated with a lower crystallinity than the single components [43]. Laboratory SWAXS and Synchrotron XRD spectra exhibited only one lamellar structure, which could be assigned to polymorph C. No further peaks were detected for blank and drug loaded NLC, which confirmed that the residual components were available in their amorphous forms. Thereby, oleic acid depressed the melting point as well as the crystallization temperature of palmitic acid and consequently, suppressed the formation of the thermodynamically less stable form. Moreover, the drug decreased the crystallization temperature of the lipid mixture, suggesting that most of the drug (98.9%) was tightly bound to the carrier matrix, while excess material (1.1%) adhered to the lipid surface as a liquid phase, further suppressing crystallinity [26]. These findings are in good agreement with Bunjes and co-workers, who reported that the incorporation of ubidecarenone into tripalmitin-based nanoparticles also reduced the crystallization temperature, suppressing crystallization [44].

Since polymorphic changes of lipids are likely to occur during storage, NLC were stored over 10 weeks and their physico-chemical stability was systematically mapped with synchrotron XRD and laboratory SAXS. The synchrotron XRD spectra showed no changes in crystallinity for drug loaded and blank NLC after 10 weeks. By contrast, laboratory SAXS spectra showed structural disorders. Over time, palmitic acid first transformed into an intermediate phase (i.e., phase between crystalline and amorphous state), which was recognizable by the weak SAXS signals, and then into an energetically more favorable state by forming a second lamellar phase (polymorph B). These results coincided with the SAXS spectra of the single component after tempering. To study if polymorph B caused morphological alterations of the encapsulated drug, structural changes of the crystallinity of the lamellar phases and/or modifications in particle shape, we performed temperature scans using synchrotron SAXS. Increasing the temperature to 69.85 °C

resulted in melting of the particles and transformation into the amorphous state. The amorphous state decreased the scattered intensity because a high scattered intensity corresponds to a high degree of crystallinity [45]. During cooling to −0.15 °C, a conversion from the amorphous to the crystalline state occurred and particle formation took place again. Both lamellar phases were detectable in the synchrotron SAXS spectrum and no drug peaks were observed. This confirms that the drug was still encapsulated in the particles in its amorphous state. Besides the lamellar structure, the scattering signal also provides information about the particle shape [22]. The scattering signal of NLC was visible in the low q range with an experimentally obtained q_{peak_max} at 0.850 nm^{-1} indicating that the particles were spherically shaped. The spherical shape did not change after several temperature scan frames, further suggesting that polymorph B did not affect the spherical particle shape during storage. To verify this assumption, we simulated the form factor according to the spherical core-shell model [21]. The form factor NLC-plot showed modulated maxima because of the bilayer shell thickness, confirming a spherical shape. The narrow spaced maxima were not taken into account because the resolution of the theoretical simulation was beyond the limit of our experimental SAXS resolution [21]. The structure factor (sharp lamellar Bragg peaks) implied that apart from being spherical, NLC showed a lamellar onion-like structure [35,46]. This can be traced back to the existence of a hydrophobic part forming the core, and a hydrophilic part referred as shell.

4. Conclusions

Currently, the most widely employed techniques to study lipid nanoparticles are PCS to measure particle size, particle size distribution and zeta potential, DSC and laboratory XRD. However, these methods are not sufficient to get a deeper understanding of the inner crystalline structure, polymorphic changes and particle shape. Since these characteristics might adversely affect the stability of a lipid drug delivery system, and consequently, the therapeutic effect of the drug, they have to be taken into account during formulation development. Here, we tested advanced methods, including laboratory SWAXS, synchrotron XRD and SAXS to establish a characterization tool and provide more accurate information on NLC after preparation and during storage. It was found that NLC incorporate the drug in its amorphous form. Synchrotron XRD spectra showed no changes in crystallinity within nine weeks. However, using laboratory SAXS a second lamellar structure, identified as polymorph B was detected. By performing synchrotron SAXS temperature scans we showed that due to heating and cooling polymorph B did not change (i) the morphological state of the incorporated drug, (ii) the crystallinity of the lamellar phases and (iii) the shape of NLC. These data highlight the unique capabilities of laboratory and synchrotron X-ray Scattering and Diffraction for improved structural characterization of lipid nanoparticles.

Acknowledgements

The authors would like to thank Heinz Amenitsch (TU-Graz), Giorgio Bais and Maurizio Polentarutti (Elettra Synchrotron Trieste) for measurements support.

This research did not receive any specific grant from funding agencies in the public, commercial, or not-for-profit sectors.

This work is part of the scientific activities of the internal CERIC-ERIC research project “Nano Analytics in Pharmaceutics”.

Appendix A. Supplementary data

Supplementary data to this article can be found online at https://doi.org/10.1016/j.ejpb.2019.03.017.

References

[1] R.H. Müller, R. Shegokar, C.M. Keck, 20 years of lipid nanoparticles (SLN & NLC): present state of development & industrial applications, Curr. Drug Discov. Technol. 8 (2011) 207–227, https://doi.org/10.2174/157016311796799062.
[2] R.H. Müller, M. Radtke, S.A. Wissing, Nanostructured lipid matrices for improved microencapsulation of drugs, Int. J. Pharm. 242 (2002) 121–128 http://www.ncbi.nlm.nih.gov/pubmed/12176234.
[3] C.W. How, R. Abdullah, R. Abbasalipourkabir, Physicochemical properties of nanostructured lipid carriers as colloidal carrier system stabilized with polysorbate 20 and polysorbate 80, African J. Biotechnol. 10 (2011) 1684–1689, https://doi.org/10.5897/AJB10.1667.
[4] D. Irby, C. Du, F. Li, Lipid-drug conjugate for enhancing drug delivery, Mol. Pharm. 14 (2017) 1325–1338, https://doi.org/10.1021/acs.molpharmaceut.6b01027.
[5] Y. Ding, K.A. Nielsen, B.P. Nielsen, N.W. Bøje, R.H. Müller, S.M. Pyo, Lipid-drug-conjugate (LDC) solid lipid nanoparticles (SLN) for the delivery of nicotine to the oral cavity – optimization of nicotine loading efficiency, Eur. J. Pharm. Biopharm. 128 (2018) 10–17, https://doi.org/10.1016/j.ejpb.2018.03.004.
[6] A. Gessner, C. Olbrich, W. Schröder, O. Kayser, R.H. Müller, The role of plasma proteins in brain targeting: species dependent protein adsorption patterns on brain-specific lipid drug conjugate (LDC) nanoparticles, Int. J. Pharm. 214 (2001) 87–91.
[7] M. Muchow, P. Maincent, R.H. Muller, Lipid nanoparticles with a solid matrix (SLN, NLC, LDC) for oral drug delivery, Drug Dev. Ind. Pharm. 34 (2008) 1394–1405, https://doi.org/10.1080/03639040802130061.
[8] C. Olbrich, A. Gessner, O. Kayser, R.H. Müller, Lipid-Drug-Conjugate (LDC) nanoparticles as novel carrier system for the hydrophilic antitrypanosomal drug diminazenediaceturate, J. Drug Target. 10 (2002) 387–396, https://doi.org/10.1080/1061186021000001832.
[9] A. Noack, G. Hause, K. Mäder, Physicochemical characterization of curcuminoid-loaded solid lipid nanoparticles, Int. J. Pharm. 423 (2012) 440–451, https://doi.org/10.1016/J.IJPHARM.2011.12.011.
[10] R. Shah, D. Eldridge, E. Palombo, I. Harding, Characterization, in: Lipid nanoparticles prod. Chartacterization Stab., Springer, Cham, 2015: pp. 45–74. 10.1007/978-3-319-10711-0_4.
[11] M. Üner, Preparation, characterization and physico-chemical properties of solid lipid nanoparticles (SLN) and nanostructured lipid carriers (NLC): their benefits as colloidal drug carrier systems, Pharmazie. 61 (2006) 375–386.
[12] K. Oehlke, D. Behsnilian, E. Mayer-Miebach, P.G. Weidler, R. Greiner, Edible solid lipid nanoparticles (SLN) as carrier system for antioxidants of different lipophilicity, PLoS One 12 (2017) e0171662, , https://doi.org/10.1371/journal.pone.0171662.
[13] M.A. Schubert, M. Harms, C.C. Müller-Goymann, Structural investigations on lipid nanoparticles containing high amounts of lecithin, Eur. J. Pharm. Sci. 27 (2006) 226–236, https://doi.org/10.1016/J.EJPS.2005.10.004.
[14] H. Bunjes, T. Unruh, Characterization of lipid nanoparticles by differential scanning calorimetry, X-ray and neutron scattering, Adv. Drug Deliv. Rev. 59 (2007) 379–402, https://doi.org/10.1016/J.ADDR.2007.04.013.
[15] D. Mitcham, A.V. Bailey, V.W. Tripp, Identification of fatty acid polymorphic modifications by infrared spectroscopy, J. Am. Oil Chem. Soc. 50 (1973) 446–449, https://doi.org/10.1007/BF02639851.
[16] E. Moreno, R. Cordobilla, T. Calvet, F.J. Lahoz, A.I. Balana, The C form of n-hexadecanoic acid, Acta Crystallogr. Sect. C Cryst. Struct. Commun. 62 (2006) 129–131, https://doi.org/10.1107/S0108270106003106.
[17] H. Bunjes, Structural properties of solid lipid based colloidal drug delivery systems, Curr. Opin. Colloid Interface Sci. 16 (2011) 405–411, https://doi.org/10.1016/J.COCIS.2011.06.007.
[18] M. Üner, Characterization and imaging of solid lipid nanoparticles and nanostructured lipid carriers, in: Handb. Nanoparticles, Springer International Publishing, Cham, 2015, pp. 1–20. 10.1007/978-3-319-13188-7_3-1.
[19] E.B. Manaia, M.P. Abuçafy, B.G. Chiari-Andréo, B.L. Silva, J.A. Oshiro Junior, L.A. Chiavacci, Physicochemical characterization of drug nanocarriers, Int. J. Nanomedicine. 12 (2017) 4991–5011, https://doi.org/10.2147/IJN.S133832.
[20] T. Li, A.J. Senesi, B. Lee, Small angle X-ray scattering for nanoparticle research, Chem. Rev. 116 (2016) 11128–11180, https://doi.org/10.1021/acs.chemrev.5b00690.
[21] O. Glatter, O. Kratky, Small angle X-ray scattering, Academic Press, London, New York, 1982.
[22] T.P. Lodge, J. Bang, Z. Li, M.A. Hillmyer, Y. Talmon, Introductory lecture: strategies for controlling intra- and intermicellar packing in block copolymer solutions: illustrating the flexibility of the self-assembly toolbox, Faraday Discuss. 128 (2005) 1, https://doi.org/10.1039/b412755m.
[23] T. Narayanan, J. Gummel, M. Gradzielski, Probing the self-assembly of unilamellar vesicles using time-resolved SAXS, Adv. Planar Lipid Bilayers Liposomes. 20 (2014) 171–196, https://doi.org/10.1016/B978-0-12-418698-9.00007-1.
[24] Y. Li, J. Zhao, Y. Qu, Y. Gao, Z. Guo, Z. Liu, Y. Zhao, C. Chen, B., U. Medicine, Synchrotron radiation techniques for nanotoxicology, Nanomedicine NBM 11 (2015) (2015) 1531–1549.
[25] D.I. Svergun, E.V. Shtykova, V.V. Volkov, L.A. Feigin, Small-angle X-ray scattering, synchrotron radiation, and the structure of bio- and nanosystems, Crystallogr. Reports. 56 (2011) 725–750, https://doi.org/10.1134/S1063774511050221.
[26] C. Tetyczka, M. Griesbacher, M. Absenger-Novak, E. Fröhlich, E. Roblegg, Development of nanostructured lipid carriers for intraoral delivery of domperidone, Int. J. Pharm. 526 (2017) 188–198, https://doi.org/10.1016/j.ijpharm.2017.04.076.
[27] J. Lyklema, Electrokinetics after Smoluchowski, Colloids Surfaces A Physicochem. Eng. Asp. 222 (2003) 5–14, https://doi.org/10.1016/S0927-7757(03)00217-6.

[28] H. Amenitsch, M. Rappolt, M. Kriechbaum, H. Mio, P. Laggner, S. Bernstorff, First performance assessment of the small-angle X-ray scattering beamline at ELETTRA, J. Synchrotron Radiat. 5 (1998) 506–508, https://doi.org/10.1107/S090904959800137X.
[29] A. Guinier, G. Fournet, Small Angle Scattering of X-rays, John Wiley and Sons, New York, NY, 1955.
[30] A. Lausi, M. Polentarutti, S. Onesti, J.R. Plaisier, E. Busetto, G. Bais, L. Barba, A. Cassetta, G. Campi, D. Lamba, A. Pifferi, S.C. Mande, S.M. Sarma, G. Paolucci, Status of the crystallography beamlines at Elettra, Eur. Phys. J. Plus. 130 (2015) 1–20, https://doi.org/10.1140/epjp/i2015-15056-x.
[31] A.P. Hammersley, FIT2D: a multi-purpose data reduction, analysis and visualization program, J. Appl. Crystallogr. 49 (2016) 646–652, https://doi.org/10.1107/S1600576716000455.
[32] P. Thareja, C.B. Street, N.J. Wagner, M.S. Vethamuthu, K.D. Hermanson, K.P. Ananthapadmanabhan, Development of an in situ rheological method to characterize fatty acid crystallization in complex fluids, Colloids Surfaces A Physicochem. Eng. Asp. 388 (2011) 12–20, https://doi.org/10.1016/J.COLSURFA.2011.07.038.
[33] R.H. Müller, S.A. Runge, V. Ravelli, A.F. Thünemann, W. Mehnert, E.B. Souto, Cyclosporine-loaded solid lipid nanoparticles (SLN): drug-lipid physicochemical interactions and characterization of drug incorporation, Eur. J. Pharm. Biopharm. 68 (2008) 535–544, https://doi.org/10.1016/j.ejpb.2007.07.006.
[34] W.A. Kasongo, J. Pardeike, R.H. Müller, R.B. Walker, Selection and characterization of suitable lipid excipients for use in the manufacture of didanosine-loaded solid lipid nanoparticles and nanostructured lipid carriers, J. Pharm. Sci. 100 (2011) 5185–5196, https://doi.org/10.1002/JPS.22711.
[35] A. Hodzic, M. Rappolt, H. Amenitsch, P. Laggner, G. Pabst, Differential modulation of membrane structure and fluctuations by plant sterols and cholesterol, Biophys. J. 94 (2008) 3935–3944, https://doi.org/10.1529/BIOPHYSJ.107.123224.
[36] H. Ali, K. El-Sayed, P.W. Sylvester, S. Nazzal, Molecular interaction and localization of tocotrienol-rich fraction (TRF) within the matrices of lipid nanoparticles: evidence studies by Differential Scanning Calorimetry (DSC) and Proton Nuclear Magnetic Resonance spectroscopy (1H NMR), Colloids Surfaces B Biointerfaces. 77 (2010) 286–297, https://doi.org/10.1016/J.COLSURFB.2010.02.003.
[37] T.S. Awad, T. Helgason, J. Weiss, E.A. Decker, D.J. McClements, Effect of omega-3 fatty acids on crystallization, polymorphic transformation and stability of tripalmitin solid lipid nanoparticle suspensions, Cryst. Growth Des. 9 (2009) 3405–3411, https://doi.org/10.1021/cg8011684.
[38] V. Jenning, A.F. Thünemann, S.H. Gohla, Characterisation of a novel solid lipid nanoparticle carrier system based on binary mixtures of liquid and solid lipids, Int. J. Pharm. 199 (2000) 167–177, https://doi.org/10.1016/S0378-5173(00)00378-1.
[39] A. Hodzic, M. Llusa, S.D. Fraser, O. Scheibelhofer, D.M. Koller, F. Reiter, P. Laggner, J.G. Khinast, Small- and wide-angle X-ray scattering (SWAXS) for quantification of aspirin content in a binary powder mixture, Int. J. Pharm. 428 (2012) 91–95, https://doi.org/10.1016/J.IJPHARM.2012.02.048.
[40] B.A. Kerwin, Polysorbates 20 and 80 used in the formulation of protein biotherapeutics: structure and degradation pathways, J. Pharm. Sci. 97 (2008) 2924–2935, https://doi.org/10.1002/jps.21190.
[41] A. Patist, S.S. Bhagwat, K.W. Penfield, P. Aikens, D.O. Shah, On the measurement of critical micelle concentrations of pure and technical-grade nonionic surfactants, J. Surfactants Deterg. 3 (2000) 53–58, https://doi.org/10.1007/s11743-000-0113-4.
[42] H. Liang, Q. Yang, L. Deng, J. Lu, J. Chen, Phospholipid-Tween 80 mixed micelles as an intravenous delivery carrier for paclitaxel, Drug Dev. Ind. Pharm. 37 (2011) 597–605, https://doi.org/10.3109/03639045.2010.533276.
[43] C.M. Keck, A. Kovačević, R.H. Müller, S. Savić, G. Vuleta, J. Milić, Formulation of solid lipid nanoparticles (SLN): the value of different alkyl polyglucoside surfactants, Int. J. Pharm. 474 (2014) 33–41, https://doi.org/10.1016/J.IJPHARM.2014.08.008.
[44] H. Bunjes, M. Drechsler, M. Koch, K.W. Research, Incorporation of the model drug ubidecarenone into solid lipid nanoparticles, Pharm. Res. 18 (2001) 287–293.
[45] A. Hodzic, M. Kriechbaum, S. Schrank, F. Reiter, Monitoring of pentoxifylline thermal behavior by novel simultaneous laboratory small and wide X-ray scattering (SWAXS) and differential scanning calorimetry (DSC), PLoS One. 11 (2016) e0159840, , https://doi.org/10.1371/journal.pone.0159840.
[46] B. Angelov, A. Angelova, S.K. Filippov, G. Karlsson, N. Terrill, S. Lesieur, P. Štěpánek, Topology and internal structure of PEGylated lipid nanocarriers for neuronal transfection: synchrotron radiation SAXS and cryo-TEM studies, Soft Matter 7 (2011) 9714, https://doi.org/10.1039/c1sm06447a.